

## **4'-Phosphopantetheine and Long Acyl Chain -Dependent Interactions Are Integral to Human Mitochondrial Acyl Carrier Protein Function**

Jaimeen D. Majmudar<sup>#\*1</sup>, Xidong Feng<sup>#2</sup>, Nicholas G. Fox<sup>3</sup>, Joseph F. Nabhan<sup>4</sup>, Theresa Towle<sup>4</sup>, Tiffany Ma<sup>4</sup>, Renea Gooch<sup>4</sup>, Christine Bulawa<sup>4</sup>, Wyatt W. Yue<sup>3</sup>, Alain Martelli<sup>#\*4</sup>

<sup>1</sup> Chemical Biology, Medicine Design, Worldwide Research and Development, Pfizer Inc., 610 Main Street, Cambridge, MA, 02139, United States

<sup>2</sup> Discovery Sciences, Worldwide Research and Development, Pfizer Inc., Eastern Point Road, Groton, CT, 06340, United States

<sup>3</sup> Structural Genomics Consortium, Nuffield Department of Clinical Medicine, University of Oxford, OX3 7DQ, United Kingdom

<sup>4</sup> Rare Disease Research Unit, Worldwide Research and Development, Pfizer Inc., 610 Main Street, Cambridge, MA, 02139, United States

# These authors contributed equally to the work

\* To whom correspondence should be addressed:

JaimeenDevraj.Majmudar@pfizer.com

Alain.Martelli@pfizer.com

## ABSTRACT

The mitochondrial acyl carrier protein (human ACPM, yeast Acp1) is an essential mitochondrial protein. Through binding of nascent acyl chains on the serine (S112)-bound 4'-phosphopantetheine (4'-PP) cofactor, ACPM is involved in mitochondrial fatty acid synthesis and lipoic acid biogenesis. Recently, yeast Acp1 was found to interact with several mitochondrial complexes, including the iron-sulfur (Fe-S) cluster biosynthesis and respiratory complexes, *via* the binding to LYRM proteins, a family of proteins involved in assembly/stability of complexes. Importantly, the interaction of LYRM proteins with Acp1 was shown to be essential in maintaining integrity of mitochondrial complexes. Although analogous data do not exist for human ACPM, recent structures show ACPM bound to LYRM proteins and suggest that acyl chains attached to the 4'-PP cofactor are required for these interactions. Here, we characterize the mitochondrial interactome of ACPM by mass spectrometry (MS) and demonstrate the crucial role of the 4'-PP cofactor in most of ACPM interactions. Specifically, we show that human ACPM interacts with endogenous Fe-S cluster complex components through binding of the LYRM protein ISD11/LYRM4. Using knockdown experiments, we determine that ACPM is essential for the stability of mitochondrial respiratory complexes I, II and III, as well as the Fe-S cluster biosynthesis complex. Finally, using native MS and a top-down MS approach, we show that C14, C16 and C18 3-keto-acyl chains on ACPM are implicated in binding to ISD11 through analysis of the recombinant ACPM-ISD11 complex. Taken together, our data demonstrate that 4'-PP- and long acyl chains-dependent interactions are essential for human ACPM function.

## INTRODUCTION

The mitochondrial acyl carrier protein, human ACPM or NDUFAB1 (yeast Acp1), is a bacterial-type acyl carrier protein essential for mitochondrial function. ACPM is involved in mitochondrial fatty acid synthesis (mFAS) and binds acyl chains via a serine (Ser112, human numbering)-bound 4'-phosphopantetheine prosthetic group (4'-PP) <sup>1</sup>. By interacting with enzymes in the mFAS pathway, ACPM serves as a soluble scaffold for *de novo* biosynthesis and elongation of fatty acids. In that respect, ACPM is essential for the synthesis of octanoate, the precursor of lipoic acid (LA), which is a required cofactor for multiple mitochondrial enzymatic complexes such as pyruvate dehydrogenase (PDH) and  $\alpha$ -ketoglutarate dehydrogenase (KGDH) <sup>1</sup>.

In addition to its role in lipoylation, yeast mitochondrial Acp1 was recently shown to interact with multiple mitochondrial complexes including the iron-sulfur (Fe-S) cluster biosynthesis complex Isu-Nfs1-Isd11 and respiratory complexes I, II and III <sup>2-4</sup>. Binding of Acp1 to multiple protein complexes seems to be mediated by the interaction with LYRM proteins, a family of proteins that play a role in assembly and stability of complexes <sup>4</sup>. In *Saccharomyces cerevisiae*, knockdown of Acp1 expression results in reduced lipoylation as well as destabilization of respiratory complexes II and III and the Isu-Nfs1-Isd11 complex <sup>2, 4</sup>, therefore suggesting that interactions of Acp1 are key to its mitochondrial function. Interestingly, the 4'-PP cofactor on Acp1 was shown to be required to maintain integrity of complexes and interaction with LYRM proteins <sup>2, 4</sup>. Although the presence of an acyl chain on 4'-PP-Acp1 was reported to be dispensable for binding to LYRM proteins, the acylated form of Acp1 was proposed to be an allosteric activator that triggers binding of LYRM proteins to their target complex<sup>4</sup>.

In human cells, the role ACPM plays in the stability and function of multiple mitochondrial complexes has not been fully investigated. However, recent investigations have shown that ACPM interacts with LYRM proteins <sup>3-9</sup> and is part of the structure of complex I <sup>5, 7</sup> and of the mitochondrial ribosome <sup>10</sup>. Furthermore, crystal structures of the human Fe-S cluster biosynthesis complex ISCU-NFS1-ISD11 expressed in *E. coli* contain bacterial Acp bound to ISD11 (LYRM4) <sup>8, 9</sup>. In some of the structures <sup>5, 7-9</sup>, the presence of long acyl chains (> C10) on ACPM was suggested to play a crucial role in binding LYRM

proteins <sup>8, 9</sup>. The length and nature of the acyl chain involved in the interaction of ACPM with LYRM proteins remains unclear. Based on mass spectrometry (MS) analysis, Boniecki *et al.* reported C14 acyl-chain for the *E. coli* Acp bound to ISD11 and at least 12 carbons were assigned in the X-ray crystal structure based on electron density <sup>8</sup>. Although Cory *et al.* also modelled C12 acyl-chains in the electron density of the NFS1-ISD11-*E. coli* ACP complex structure, gas chromatography MS (GC-MS) analysis detected C16 acyl-chains as the primary component and longer (>C16) acyl chains were also detected <sup>9</sup>. In a different study, electrospray ionization (ESI) MS analysis of the recombinant human ACPM-ISD11 complex showed a mixture of acylated ACPM with peaks assigned to C14, C16 and longer acyl-chains <sup>11</sup>. In the present work, we report the landscape of human ACPM interactions in a human cell line and provide supporting evidence for the importance of ACPM interactions using complementary biological and biophysical approaches. We performed a comparative MS analysis of ACPM wild-type and ACPM (S112A) mutant interactomes in HEK293T cells to evaluate the requirements of the 4'-PP cofactor for ACPM interactions. In parallel, using knockdown experiments in cells, we demonstrated the role of ACPM in maintaining the integrity of several mitochondrial complexes. Finally, using the human recombinant ACPM-ISD11 complex and native and top-down mass spectrometry analyses, we provided an unprecedented detailed structure of the major intermediate acyl-chains involved in the complex formation.

## EXPERIMENTAL

### Cloning and production of recombinant proteins

For eukaryotic expression, human ACPM (NM\_005003.2), human ACPM(S112A), ISD11 (aka LYRM4, NM\_020408.5), ISCU (NM\_213595.3) and FXN (NM\_000144.4) cDNAs were synthesized (Genewiz, South Plainfield, NJ) with a FLAG- or HA-tag sequence added on the C-terminal end and were cloned into pcDNA3.1/Hygro (-) plasmid (Invitrogen).

For bacterial expression, a DNA fragment encoding His-tagged ACPM ( $\Delta$ 1-68) and untagged ISD11, separated by an in-frame ribosomal binding site, was sub-cloned into the pNIC28-Bsa4 vector (GenBank

ID: EF198106). ACPM and ISD11 variants were constructed using the primer extension PCR method for mutagenesis and confirmed by sequencing the plasmid DNA. BL21(DE3)-R3-pRARE2 cells transformed with the above plasmids were grown in 100 mL autoinduction media (Formedium) and grown for 4 hours at 37 °C and then overnight at 22 °C. Alternatively, constructs of His-tagged human ISD11 subcloned into the pNIC28-Bsa4 vector (GenBank ID: EF198106) and untagged ACPM ( $\Delta$ 1-68), subcloned into the restriction enzyme site of the pCDF-LIC vector between NdeI and XhoI, were co-transformed for recombinant *E. coli* expression using BL21(DE3)-R3-pRARE2 cells. Cells transformed with the above plasmids were grown in Terrific Broth and induced with 0.1 mM isopropyl  $\beta$ -D-1-thiogalactopyranoside (IPTG) for 16 hours at 18 °C. Cell pellets were resuspended in binding buffer (50 mM HEPES pH 7.5, 500 mM NaCl, 20 mM Imidazole, 5% glycerol, and 2 mM TCEP) containing EDTA-free protease inhibitor (Merck), and lysed by sonication. The clarified supernatant was incubated with 2.5 mL Ni Sepharose 6 fast flow resin (GE Healthcare), washed and eluted with binding buffer containing 40 mM and 250 mM Imidazole, respectively. To isolate the complex, elution fractions were collected and loaded onto gel filtration (Superdex S75; GE Healthcare). Peak fractions were collected, treated with His-TEV protease to remove His-tag, and then passed onto Ni Sepharose 6 fast flow resin to remove His-TEV and cleaved His-tag. Fractions containing target protein were collected and buffer exchanged into gel filtration buffer (50 mM HEPES pH 7.5, 200 mM NaCl, 5% glycerol, and 2 mM TCEP). 20  $\mu$ L of sample was added to an SDS-PAGE Gel for quality of protein assessment. For pulldown experiments, samples were incubated with His-TEV protease to remove His-tag and then run on SDS-PAGE for analysis of complex formation.

### **Cell culture and transfection**

Human embryonic kidney (HEK) 293T cells (obtained from ATCC) were maintained in Dulbecco's modified Eagles's medium + GlutaMAX-I (4.5g/L D-Glucose, 110 mM Sodium Pyruvate) (Gibco, 10569-010) supplemented with 10% fetal bovine serum and 20 mM HEPES (Gibco, 15630-080) at 37 °C in a 5% CO<sub>2</sub> atmosphere. On-Target Plus siRNAs, as well as non-targeting (NT) control siRNA (D-

001500-01-05), were purchased from Dharmacon: siACP (L-019897-01), siISCU (L-012837-01), siLIAS (L-010023). Transfection was performed using DharmaFECT-1 transfection reagent (Dharmacon, T-2001-03) using manufacturer's recommendations and a final siRNA concentration of 20 nM. HEK293T cells were seeded at a density of  $3 \times 10^5$  cells in 6-well plates. Cells were harvested 72 hours after transfection for protein extraction. For immunoprecipitation experiments, cells were seeded at  $2 \times 10^6$  cells per 10-cm dish and transfected with 5  $\mu$ g of pCDNA3.1 construct using Fugene Reagent 6 (Promega, E269A) and following manufacturer's recommendations.

### **Immunoprecipitation**

Immunoprecipitations were carried out using mitochondrial-enriched protein extracts from transfected HEK293T cells (5x10-cm dishes per construct). About 40 hours after transfection, cells were harvested by scrapping plates in 1 mL PBS and by centrifuging at 500g for 5 min. Mitochondrial-enriched fraction was obtained by incubating cell pellet in 1 mL of MitoBuffer (Tris-HCl 100 mM, pH 7.5, 10% glycerol supplemented with 0.014% digitonin) at 4 °C for 10 min, and by centrifuging the suspension 10,000g 10 min at 4 °C. The resulting pellet was re-suspended in 500  $\mu$ L PEBA (Tris-HCl 10 mM pH 7.4, 10% glycerol, 100 mM NaCl, 50 mM KCl) supplemented with Complete protease inhibitor cocktail (Roche, 04693159001) and 0.2% Triton X-100, incubated 20 min on ice and centrifuged 10,000g 10 min at 4 °C. The resulting supernatant corresponding to the mitochondria-enriched protein extract (0.6-1 mg total protein) was incubated with 50  $\mu$ L EZview red beads (Sigma, anti-HA E6779 or anti-FLAG F2426) in a final volume of 1 mL PEBA. Suspension was incubated 3-4 h at 4 °C with constant mixing, centrifuged 10 min at 10,000g and beads were washed twice with 1 ml PEBA. Beads were incubated 5 min with 100  $\mu$ L glycine buffer (0.1 M glycine, pH 2.8), transferred on a micro Bio-Spin<sup>TM</sup> column (Bio-Rad, 64075460) and centrifuged for 1 min at 1,000g to collect the eluate in a 1.5 mL tube containing 10  $\mu$ L of 1M Tris-HCl, pH 8.

### **Protein extraction and immunoblotting**

Cells transfected with siRNAs were harvested and washed once with 1 mL Phosphate Buffer Saline (PBS). Pellets were extracted with 100  $\mu$ L of 50 mM Tris-HCl pH 7.5, 150 mM NaCl, 0.2% NP40 supplemented with Complete inhibitor cocktail (Roche). After a 15 min incubation on ice, suspensions were centrifuged 10,000g at 4 °C for 10 min and protein concentrations were determined using the supernatant and Pierce® 660 Protein Assay reagent (Thermoscientific, 22660). A volume of Protein Sample Buffer (150 mM Tris-HCl pH 6.8, 25% glycerol, 5% SDS) was added to samples and a brief sonication (Branson digital sonifier 450, 25% amplitude; 0.2s on/off pulses, 10 rounds) was performed to mix pellet and supernatant and obtain protein extracts containing membrane proteins. Extracts were heated at 100 °C for 5 min and NuPAGE LDS sample buffer (Invitrogen, NP0007) supplemented with 1% 2-mercaptoethanol was added. Samples (5  $\mu$ g total protein) were run on 4-12% NuPAGE Bis-Tris gels (Invitrogen, WG1402BX10) using MES running buffer (Novex, NP0002) and transferred on nitrocellulose membrane (Bio-Rad, Trans-blot Turbo Transfer Pack, 170-4159). After blocking in 5% nonfat milk (Cell Signaling, 9999S), TBS-Tween (0.05%) (TBS-T) for at least 1 hour, membranes were incubated with primary antibodies in 5% nonfat milk TBS-T overnight at 4 °C: anti-ACPM (NDUFAB1, Abcam ab181021, 1/1,000); anti-ISD11 (Novus Biologicals, NBP1-79672, 1/1,000); anti-ISCU (Abcam ab180532, 1/1,000); anti-NFS1 (Proteintech 15370-1-AP, 1/1,000); anti-SDHB (Abcam ab14714, 1/6,000); anti-RIESKE (UQCRRFS1, Abcam ab14746, 1/4,000); anti-NDUFS3 (Invitrogen 459130, 1/1,000); anti-lipoic acid (Calbiochem 437695, 1/6,000); anti-PDH-E2 (Abcam ab172617, 1/2,000); anti-FECH (Abcam ab137042, 1/1,000); anti-ACO2 (Abcam ab129069, 1/10,000); anti-COX2 and anti-NDUFB8 (Mitoprofile, Abcam ab110411, 1/2,000); anti-vinculine (Abcam ab207440, 1/1,000); anti-HA-HRP (Sigma H6533 1/1,000); anti-FLAG-HRP (Sigma A8592, 1/6,000). Membranes were washed 4x 5 min with TBS-T, incubated with secondary antibody for 1 hour at RT (Goat anti-Mouse-HRP, Life technologies, G21040, or Goat anti-Rabbit-HRP, Life technologies, 656120, 1/7,500 in TBS-T) and washed again 4x 5 min with TBS-T. Signal was revealed using SuperSignal west Pico substrate (Thermoscientific, 34580), SuperSignal west Femto substrate (Thermoscientific, 34095) or ECL Prime reagent (GE Healthcare, RPN2232) and exposed on films (Amersham Hyperfilm ECL, 45001508).

### **RNA extraction and droplet digital PCR**

RNA was extracted using RNeasy mini kit (Qiagen, 74106) following manufacturer's protocol. Reverse transcription was performed using 1 µg total RNA and the iScript cDNA synthesis kit (Bio-Rad, 1708891). Expression levels were determined using ddPCR Supermix for probes (Bio-Rad, 186-3027) as well as the Bio-Rad QX200 droplet generator and droplet reader. Specific probes and primers sets were ordered from Life technologies: FAM-probes of ACP (NDUFAB1, Hs00900741\_g1), ISCU (Hs00384510\_m1), LIAS (Hs01567818\_m1), and VIC-probe of TBP (Hs99999910\_m1) as control.

### **Liquid chromatography mass spectrometry (LC-MS) analysis of co-immunoprecipitation samples**

Eluted proteins obtained from immunoprecipitation (see immunoprecipitation section) were first dried using a speed vac (Thermo Savant SPD131DDA) for 45 minutes at 45 °C. Dried control and bait samples were then re-suspended in 30µL of freshly prepared 6M urea/PBS. Samples were treated with dithiothreitol (D0632, Sigma-Aldrich, 5mM final concentration) for 45 minutes at 37 °C followed by 20mM final iodoacetamide concentration (I1149, Bio-Ultra, Sigma-Aldrich, 45 minutes, room temperature, dark). Each sample was then diluted by adding 120 µL of freshly prepared 62.5 mM ammonium bicarbonate (A6141, Sigma-Aldrich) containing 1mM calcium chloride (BP510-100, Fisher Scientific) to a final volume of 150 µL. Pull-down samples were then digested with 2µg MS-grade Trypsin/LysC mix (V5073, Promega) for 12 hours at 37 °C. Digested peptides were then desalted using C-18 spin columns (Pierce-Thermo Scientific, 89870) following the manufacturer's instructions. Desalted peptides were eluted using LC-MS optima grade 70% acetonitrile in water (25µL, 2x) and dried using a speed vac. Dried, desalted peptides were then re-suspended in 15 µL of LC-MS Optima grade 5% acetonitrile in water containing 0.1% formic acid. The samples were analyzed by one-dimensional liquid chromatography tandem mass spectrometry, using a Q Exactive Orbitrap mass spectrometer (Thermo Scientific) coupled to a Thermo Easy nLC 1000. The peptides were then loaded onto a trap column (Acclaim PepMap 100 C18 trap column, 75 µM x 2cm nanoViper, P/N 164946) at a flow rate of 20



μL/min. Peptides were eluted using a 50-cm C18 column (Thermo Scientific ES803) over 120 minutes using a gradient of 5-40% buffer B (20% water, 80% acetonitrile, 0.1% formic acid) in buffer A (99.9% water, 0.1% formic acid). Data was collected in data-dependent acquisition mode with dynamic exclusion enabled (30s, repeat count of 2). One full MS (MS1) scan ( $m/z$  350-1600) was followed by top 15 MS2 scans. Peptide identification of the spectra performed using Mascot. Each MS2 spectra were searched using the Mascot algorithm against a reverse concatenated, non-redundant database of the human proteome (UniProt release–January 2017).

### **Proteomics Data processing post acquisition**

Data obtained from label-free quantification were uploaded in SpotFire and then filtered for the following criteria (1) Minimum 3 peptides (2) Minimum 5 Peptide Spectral Matches (PSMs) (3) Minimum fold-change of 3 (4) Quantified in both biological replicates (5) Have a p-value of less than or equal to 0.05, and (6) Less than 15% probability of being a contaminant as analyzed through the Contaminant Repository for Affinity Purification (CRAPome.org) <sup>12</sup>. Finally, hits were selected based on their mitochondrial localization as defined by MitoCarta 2.0 <sup>13</sup>. Each immunoprecipitation experiment had 2 biological replicates (except the ACPM S112A experiment, which had 4 biological replicates). Only proteins that were identified as hits in both sets of biological replicates and met the filtering criteria are considered as true hits, or interaction partners. Proteins that were detected only in the sample and not in the control (infinite fold change) were arbitrarily assigned a fold-change value of 100.

### **LC-MS analysis of 4'-PP conjugated acyl-chains**

Mass measurement was carried out utilizing the Synapt G2 HDMS (Waters, Milford, MA) instrument equipped with Lockspray system, quadrupole mass analyzer, trap collision cell, and time-of-flight mass analyzer in tandem. Liquid chromatography was carried out using an ACQUITY UPLC system with a PLRP column at a flow rate of 0.30 ml/min. The MS/MS/MS measurement on the acyl-chain conjugated with 4'-PP were conducted first by ejecting them from ACPM in the ion source region through in-source

CID, and then being fragmented by trap CID after selection in the quadrupole. The instrument was externally calibrated using NaI solution and each spectrum was internally calibrated further through lock-mass calibration using leucine enkephalin at  $m/z$  556.2771<sup>+</sup> for both the intact mass measurement and the tandem MS measurement with mass accuracy of a few ppm routinely achieved.

Waters MassLynx software (Versions 4.1) was used for data acquisition and analysis, including calculations of predicted masses and simulation of isotopic distributions. The mass measurement errors ( $\Delta$ ) are the differences between the experimental and predicted values expressed in mDa, or when divided by the predicted mass in ppm units. All calculated ion masses do not include corrections for the mass of the electrons responsible for the charge state of the ion.

#### **Native MS analysis of the ACPM-ISD11 complex**

In native MS measurements, the ACPM-ISD11 protein complex sample was first buffer exchanged into 200 mM ammonium acetate buffer with pH7.5 using Amicon centrifugal filters with cutoff of 3 kDa, and then ~5  $\mu$ L sample was loaded into an offline electrospray capillary (GlassTip 4  $\mu$ m i.d.; New Objective, Woburn, MA). High voltage 1.0–1.5 kV was applied together with a low pressure gas at the back end of the capillary to start and maintain a stable spraying directly into the mass spectrometer. The hybrid ion-mobility quadrupole time-of flight mass spectrometer (SYNAPT G2 HDMS; Waters, Milford, MA) was used and operated in the sensitivity mode with ESI source parameters tuned to preserve the protein complexes intact and meanwhile to maintain decent sensitivity. MS/MS measurement on the protein complex was carried out using CID in the trap region with elevated trap potential after selection in the quadrupole. Some critical parameters for good native MS measurement are source temperature 40 °C, sampling cone 60-80 V, trap potential 5V, and backing pressure of 5–6 mbar. The instrument was externally calibrated using CsI solution for up to  $m/z$  8000, and the data processing was performed using MassLynx (ver. 4.1, Waters).

## **RESULTS & DISCUSSION**

#### **4'-Phosphopantetheine-dependent interactome of human ACPM**

We first performed a comprehensive analysis of the ACPM mitochondrial interactome and interrogated the role of the 4'-phosphopantetheinylation in ACPM interactions. Immunoprecipitation (IP) experiments were carried out using enriched mitochondrial fractions of HEK293T cells transiently transfected with ACPM-Flag or with a ACPM(S112A)-Flag construct that yields a non-4'-phosphopantetheinylated form of ACPM protein. Two replicate samples per construct were analyzed by liquid chromatography – MS (LC-MS) and label-free quantification was carried out using non-transfected cells as controls. We appreciate the caveats of utilizing tagged systems to perform co-immunoprecipitation experiments as these can sometimes interfere with interaction partners and also result in some false-positives. To avoid these pitfalls, we cross-matched our data with common contaminants as defined by the contaminant repository for affinity purification as one of our filters and only allowed proteins that have less than 10% probability of being a contaminant as a “hit”. Furthermore, working with small proteins such as ACPM and ISD11 poses additional complications, as antibody binding sites may often occlude binding sites for true interactors. An example that justifies this finding is the striking example by Schmucker et al. where the monoclonal 1G2 antibody to frataxin interfered in its interactions with NFS1 and ISCU. **[NEED REF]**

Using thresholds defined in the Experimental section, we identified 72 mitochondrial interaction partners of wild-type ACPM (Figure 1, supplementary Table 1). In agreement with previously reported data <sup>6</sup>, interactions with LYRM proteins were detected (Table 1, supplementary Table 1): LYRM2, LYRM3 (NDUFB9), ISD11 (LYRM4), LYRM6 (NDUFA6), LYRM7 (MZM1L), LYRM8 (SDHAF1), ACN9 (SDHAF3) and C7orf55 (FMC1). Although LYRM5 (ETFRF1) could be detected in both biological replicates with a fold change of 100, it did not meet the criteria of a minimum of 3 unique peptides to be considered as a hit. However, ETFA and ETFB, which are direct partners of LYRM5 <sup>6</sup>, were identified as interactors of ACPM (supplementary Table 1), hence indirectly supporting binding of ACPM to LYRM5. Interaction of ACPM with several members of the mitochondrial electron transport chain was also observed. Specifically, subunits of Complex I (NDUFS1, NDUFS7), Complex II (SDHB), Complex III

(UQCC2 and UQCRFS1) and Complex V (ATP5H aka ATP5PD or ATP5J2) were detected, whereas no interaction with complex IV subunits was observed. It is possible that ACPM interactions with the members of the mitochondrial electron transport chain are mediated by LYRM proteins involved in assembly and stability of the different respiratory complexes (Table 1, supplementary Table 1). Our current data do not point to a model where ACPM interacts with transport chain proteins through LYRM proteins, but follow-up co-immunoprecipitation experiments of various LYRM proteins could shed light on the link between ACPM, electron transport chain components and LYRM proteins.

The identification of LIPT2, which catalyzes the transfer of octanoate from octanoyl-ACP onto lipoyl domains of lipoic acid-dependent enzymes, and GLDC, a lipoic acid dependent enzyme, as hits in ACPM IPs pointed to the role of ACPM in lipoic acid synthesis. Furthermore, OXSM (3-oxoacyl-[acyl-carrier-protein] synthase) was the only enzyme of mFAS to be found as an interaction partner of ACPM (Table 1, supplementary Table 1).

Twenty four mitochondrial ribosomal proteins (MRPL proteins) were also identified as hits in ACPM IPs (supplementary Table 1). This finding is consistent with the recent identification of ACPM as part of the human mitochondrial ribosome structure <sup>10</sup>.

In addition to the LYRM protein ISD11, NFS1 and ISCU were also found as hits in the ACPM IPs by LC-MS. The presence of NFS1 in ACPM IP was further assessed by western blot and compared with detection in the IPs of the scaffold protein ISCU (ISCU-Flag), ISD11 (ISD11-HA) and frataxin (FXN-HA), a partner and allosteric regulator of the ISCU-NFS1-ISD11 complex <sup>14-16</sup>. As expected, NFS1 was detected in FXN-HA, ISCU-Flag and ISD11-HA IPs, and was also observed in ACPM-Flag IP (Figure 2A), hence confirming binding of ACPM to the Fe-S cluster biosynthesis complex. To identify the interaction partner of ACPM within the complex, FXN-HA, ISCU-Flag and ISD11-HA IPs were analyzed using an ACPM-specific antibody (Figure 2B). No ACPM signal could be detected in the FXN-HA IP (Figure 2B), suggesting that their interaction is not direct. Although NFS1 signal was similar between ISCU-Flag and ISD11-HA IPs, a strong signal of ACPM was only seen in ISD11-HA IP (Figure 2B), thus

supporting the binding of ACPM to ISD11. The interaction of ACPM with ISD11 was also observed by unbiased LC-MS analysis of the ISD11-HA IP since ACPM was detected in addition to NFS1, ISCU and FXN (supplementary Table 2). Therefore, similar to what was reported for yeast Acp1<sup>2, 4</sup>, our data indicate that human ACPM is an integral part of the endogenous Fe-S cluster biosynthesis complex *via* the interaction with the LYRM protein ISD11.

In such a co-immunoprecipitation study to identify interaction partners of ACPM, enzymes involved in ACPM biosynthesis (MCAT, OXSM, HSDL2, HTD2 and MECR) were expected to be identified as interaction partners of ACPM. Of these, only OXSM was identified as an interaction partner that met all our filtering criteria. We detected 3 others in our initial list (MCAT, HSDL2 and MECR), but were triaged as they did not pass one filter (minimum 3 peptides or the *p-value* threshold). This highlights a shortcoming of utilizing strict thresholds to determine interaction partners in a proteomic analysis, and suggests that proteins identified with 1-2 unique peptides (or ones with *p-values* greater than 0.05) may still be bona-fide interactors of the bait in question. This retrospective analysis gives us a much higher confidence in our final list of ACPM interaction partners as even some of our “medium-confidence” hits are likely biologically relevant interaction partners of ACPM. We encourage the readers of this manuscript to use our dataset as a starting point to identify interaction partners of ACPM, and keep in mind that of the hits that did not make the final list may still be (weak) interaction partners of ACPM.”

When mutant ACPM(S112A)-Flag was used as bait, the majority of the interactions detected with WT ACPM were lost including subunits of complex I, II, III, the MRPL proteins and components of the Fe-S cluster biosynthesis complex (Figure 3, Supplementary Table 3). The inability of ACPM(S112A) to bind to the Fe-S cluster biosynthesis complex was further confirmed by western blotting since NFS1 could not be detected in the ACPM(S112A)-Flag IP (Figure 2A).

Only two hits were retained with ACPM(S112A): TRMT2B (SAM-dependent methyl transferase on tRNA) and ATPAF2 (assembly of F1 component of the mitochondrial ATP synthase) (supplementary

Table 3). Intriguingly, S112A-ACPM retained its ability to interact with ATPAF2, which is the human homolog of Atp12, an assembly factor of the F1 sector of ATP synthase. In yeast, the LYR protein Fmc1 binds Atp12, and indeed, while we did detect FMC1 (C7orf55) as a putative interacting partner of S112A-ACPM, FMC1 was detected with only a single peptide; which did not meet all our filtering criteria. This raises an interesting possibility that ACPM lacking the 4'PP cofactor retains its ability to interact with LYR protein FMC1 and also with ATPAF2. This hypothesis regarding the role of ACPM lacking the 4'PP cofactor needs to be further probed into as it raises several questions regarding the biological function of non-phosphopantetheinylated ACPM. While S112A-ACPM lost most of its interaction partners, seven new mitochondrial protein partners were identified in ACPM(S112A) IPs: CHCHD7, GBAS, HEBP1, NDUFA5, PSAP, SLIRP and TRMT61B (Supplementary Table 3). This suggests that under a non-phosphopantetheinylated state (if such state exists under biologically relevant conditions), ACPM may display a unique set of interactions and function distinct from the ACPM holoprotein.

Together, our data demonstrate the crucial role of 4'-PP cofactor in the interaction of ACPM with essential mitochondrial proteins and complexes.

### **Human ACPM contributes to the integrity of multiple essential mitochondrial complexes**

To mimic the loss of ACPM interactions and understand how these interactions contribute to the activity and stability of different mitochondrial complexes and pathways, we conducted ACPM knockdown (KD) experiments in HEK293T cells. The abundance of protein components of multiple mitochondrial respiratory complexes, Fe-S cluster proteins and protein-conjugated lipoic acid (LA) was assessed by western blotting as an indirect evaluation of complex integrity and activity<sup>17, 18</sup>. Knockdown efficiency was confirmed by western blotting and/or by measuring mRNA expression of the targeted gene (Figure 4, supplementary Figure 1). As expected due to its role in LA biosynthesis, levels of lipoylated pyruvate dehydrogenase (PDH) and  $\alpha$ -ketoglutarate dehydrogenase (KGDH) were drastically reduced upon ACPM KD (Figure 4). Furthermore, a clear decrease in complex I (NDUFS3 and NDUFB8), complex II (SDHB) and complex III (RIESKE) subunits was observed, whereas no effect on complex IV subunit COX2 was

seen (Figure 4). These decreased levels mirror our interactome proteomics experiments in which interactions with complex I, II and III subunits were detected in ACPM IP, whereas no protein of complex IV was identified (Figure 4), and therefore suggest that the ACPM interaction is required to maintain the integrity of these respiratory complexes.

Interestingly, ISCU and, to a lesser extent, NFS1 protein levels were reduced by ACPM KD when compared to control (Figure 4). Since complexes I, II, and III are Fe-S cluster-containing complexes, one could hypothesize that the effect of ACPM KD on respiratory complexes could be an indirect consequence of general Fe-S biogenesis impairment triggered by ISCU-NFS1-ISD11 instability (Figure 4). To test a potential indirect effect, KD of ISCU, the scaffold protein required for Fe-S cluster synthesis, was performed in parallel. As previously reported <sup>17</sup>, ISCU KD triggered a significant decrease of components of all Fe-S cluster-dependent respiratory complexes (NDUFS3, NDUFB8, SDHB, RIESKE) and of lipoylated PDH and KGDH levels due to the impairment of lipoic acid synthase (LIAS), a Fe-S cluster-containing enzyme (Figure 4). ISCU KD also led to a strong decrease of ferrochelatase (FECH) and to a lesser extent of mitochondrial aconitase (ACO2), two Fe-S cluster enzymes that were not seen to interact with ACPM (Figure 4). No decrease of FECH and ACO2 protein levels was seen in ACPM KD (Figure 4), hence indicating that the impact of ACPM KD on respiratory complexes relates to its ability to interact with complexes rather than an indirect effect on Fe-S cluster synthesis. While it is not possible directly correlate ACO2 and FECH steady-state levels to their respective activities upon ACPM KD, further studies that focus on these questions would shed more light on the role of ACPM on enzymatic activities of these critical metabolic enzymes. It is also worth noting that a significant increase in ACPM protein level was observed upon ISCU KD (Figure 4). Although the biological significance of such increase remains to be defined, it further implies functional interaction between ACPM and the mitochondrial Fe-S cluster biosynthesis complex.

To test whether decrease of lipoylation could be a trigger for the mitochondrial complex instability upon ACPM KD, KD of LIAS was carried out. As expected, KD of LIAS led to a deficit in lipoylation, similar to ACPM KD, but had no effect on Fe-S cluster components and respiratory complexes (Figure 4), hence

strongly suggesting that disruption of lipoylation has no impact on mitochondrial complexes I, II, and III or the Fe-S cluster biosynthesis complex.

Together, our data indicate that interaction of ACPM is crucial for the integrity of the mitochondrial Fe-S cluster biosynthesis complex and respiratory complexes I, II and III. These data are in agreement with recent reports in yeast *S. cerevisiae* where Acp1 KD leads to decrease of complex II and III abundance and ISCU-NFS1-ISD11 instability<sup>2,4</sup>.

### **Human ACPM-ISD11 complex can be isolated by co-expression in *E. coli***

To further investigate ACPM interaction with LYRM proteins, we focused on the ACPM-ISD11 complex. Both proteins (one His-tagged, one untagged) were co-expressed in *E. coli*. The interaction between ACPM and ISD11 was observed when His-tagged ACPM pulled down untagged ISD11 in affinity chromatography (Figure 5) or when His-ISD11 was co-purified with untagged ACPM (Supplementary Figure 2A). The recombinant complex was further characterized by site-directed mutagenesis of ACPM and ISD11. Based on recently determined structures of the human ISCU-NFS1-ISD11 complex isolated with *E. coli* Acp bound to ISD11<sup>8,9</sup>, we generated a model of the human ACPM-ISD11 complex (Supplementary Figure 2B) and residues on ACPM and ISD11 were selected for mutagenesis on the basis of their location within or close to the interaction surface. The corresponding variant proteins were subjected to pulldown experiments after co-expression in *E. coli* as with wild-type. Pulldowns were analyzed by western blotting and coomassie blue staining for the presence of ISD11 and ACPM (Figure 5, Supplementary Figure 2C, D). In agreement with the IP experiments performed in HEK293T cells (Figure 2A), ACPM(S112A) variant was unable to bind ISD11 (Figure 5A). In addition, alanine substitution of D114, M120, E123 or D132 had a significant effect on complex formation (Figure 5A). On the other hand, substitutions on selected ISD11 residues had diverse effects. Some of them (Y13A, R29A, F40A and LYR/ASA) had an impact on ISD11 expression/stability since no clear signal was detected in the inputs (Figure 5B), therefore preventing assessment of their role in complex



formation. Others (R6A, L12A, R37A and R41A) clearly affected binding of ISD11 to ACPM, whereas a minor effect was seen with R14A, F23A and K44A substitutions (Figure 5B).

Altogether, our data suggest that the recombinant human ACPM-ISD11 complex recapitulates observations made in cells (this manuscript) and displays interaction features similar as the ones reported for the *E. coli* Acp-human ISD11 interaction <sup>8,9</sup> (Supplementary Figure 2B).

### **Structure of the 4'-PP conjugated fatty acyl chains in human ACPM-ISD11 complex**

The 4'-PP cofactor is essential for the attachment of fatty acyl chains onto ACPM. The involvement of long acyl chains (>C10) for the interaction of ACPM with some LYRM proteins such as ISD11 was first evidenced in the crystal structure of complex I <sup>5</sup>. To better define which acyl chains are involved in mediating the ISD11-ACPM interaction, we performed a thorough analysis of the recombinant human ACPM-ISD11 complex using native ESI-MS, which has emerged as a powerful tool for revealing the stoichiometry and subunit architecture of protein complexes <sup>19</sup>. Major ACPM components forming complexes with ISD11 were first identified through native ESI-MS analysis, followed by detailed high resolution structure elucidation of the 4'-PP-acyl chains attached to ACPM using a standard LC-MS/MS top-down approach <sup>20</sup>.

Using native ESI-MS analysis, ACPM-ISD11 protein complex was detected as a mixture of ACPM monomer, ACPM-ISD11 heterodimer and hetero-tetramer (Figure 6A). The detection of the heterodimers and the heterotetramer detected is likely not a function of higher protein concentrations, as these experiments were run at a low protein concentration of 10-20μM. At these lower concentrations, the probability of identification of higher order structures as artifacts of protein concentration are eliminated. Both ACPM-ISD11 heterodimer and hetero-tetramer were further characterized by collision-induced dissociation (CID) with each individual monomer component ejected and measured to confirm the assignments (Supplementary Figure 3). The heterodimer and tetramer peaks were broad due to the heterogeneity of ACPM tethered with various lengths of acyl-chains, as well as the co-existence of both intact and truncated ISD11 forms (see below). However, the ACPM-ISD11 heterodimer peaks with

different acyl-chain lengths were resolved and could be attributed to ACPM with C14, C16 and C18 3-ketoacyl-chain (Figure 6B).. A heterodimer with a short C4 saturated acyl-chain was also detected but with much lower abundance (Figure 6B). Conversely, the major ACPM monomer detected in the same spectrum was with the 4'-PP conjugated with short C4 saturated acyl-chain and no 3-ketoacyl-chain with C14, C16, and C18 was detected (Figure 6B). Although the 4'-PP conjugated ACPM monomer without any acyl-chain was detected ( $m/z$  1752.5 Da), the heterodimer and hetero-tetramer containing that form in complex with ISD11 were not detected, suggesting that hardly any complex can be formed in the absence of an acyl chain on ACPM. Our results contrast with the recent report in *S. cerevisiae* in which interaction of 4'-PP-Acp1 with Isd11 could be observed by pulldown without requiring the acyl chain for binding <sup>4</sup>.

To further confirm the structural assignments on the individual components of the ACPM-ISD11 complex, a standard LC-MS analysis was carried out. Intact ISD11 was detected with a mass of 10829 Da (Supplementary Figure 4A). In addition, a truncated form of ISD11 (ISD11<sub>tr</sub>) with a mass of 9058 Da was detected as the major ISD11 species (Supplementary Figure 4A). Four major components were detected for ACPM with masses of 10580/10734/10761/10790 Da (Supplementary Figure 4B), and all four components were with similar relative abundance based on UV absorbance (Supplementary Figure 5).

To obtain a more detailed structure of the acyl chains bound to ACPM in the ACPM-ISD11 complexes, top-down MS/MS with CID was applied to each of the isolated major ACPM components. Facile elimination of the 4'-PP-acyl chain in the gas phase was observed, as previously reported <sup>20</sup>. The eliminated 4'-PP acyl chains were subsequently detected in the full MS and tandem MS modes with ppm accuracy (Figure 7A). Unique elemental composition could be readily established as C<sub>11</sub>H<sub>21</sub>N<sub>2</sub>O<sub>3</sub>S<sup>+</sup> for the abundant shared fragment ion  $m/z$  261.127 based on accurate mass (Pred, 261.127,  $\Delta$ =0 mDa) and sulfur isotope ratio (<sup>34</sup>S/<sup>32</sup>S, ~4%). The sub-structure for the ion at  $m/z$  261.127 could be easily assigned as derived from the eliminated 4'-PP with cleavage of the thioester bond (Figure 7A). This assignment was further supported by the detection of another shared fragment ion  $m/z$  184.098 (Pred, 184.097,  $\Delta$ =1 mDa) resulting from the cleavage of the amide bond (Figure 7A). Complementary fragment ions to  $m/z$

261 were not detected due to the lack of charge on the acyl-chain. However, unique elemental compositions for the various acyl-chains could be directly derived from the neutral loss with ppm accuracy and assigned to saturated C4, 3-keto-C14, 3-keto-C16 and 3-keto-C18 acyl chains (Figure 7B). The accuracy (~1 ppm) of our MS analysis was sufficient to rule out the saturated acyl-chain structures. Due to lack of cleavage along the acyl-chain, the structures were proposed based on the known formation of 3-keto-acyl intermediates during mFAS, which is catalyzed by the 3-oxoacyl-ACP synthase (OXSM)<sup>1</sup>. Interestingly, the identification of OXSM as one of the protein partners of ACPM in our proteomic analysis (Table 1, supplementary Table 1) suggests that this interaction and specific mFAS reaction might play an important role in ACPM and related mitochondrial functions.

The measured nominal mass for ACPM agreed well with the predicted mass based on the proposed 4'-PP conjugated acyl-chains. Furthermore, the isotopes were resolved with mass accuracy of a few ppm achieved for each of the abundant isotopes, and mapping the isotopic distributions of ACPM with the proposed 4'-PP conjugated acyl-chains over the observed data showed good agreement (Figure 7C).

Together, our findings indicate that 4'-PP-conjugated ACPM with longer acyl-chains (C14, C16 and C18) are primarily involved in the interaction with ISD11. These data are consistent with recent crystallography findings suggesting that acyl-chains were docked into the ISD11 hydrophobic core and that longer acyl-chains favor stronger interaction<sup>8,9</sup>.

## CONCLUSIONS

In summary, our analysis of human ACPM mitochondrial interactions point to a model where structural integrity of multiple mitochondrial complexes such as the Fe-S cluster biosynthesis complex and respiratory complexes I, II, III are dependent on ACPM that is modified by the 4'-PP prosthetic group. Furthermore, our high-resolution native MS studies on the ACPM-ISD11 complex showed that this specific interaction is likely mediated by long 3-keto acyl chains (C14, C16 and C18). This may be true for other ACPM-LYRM protein interactions, but further investigations are required with particular attention to acyl chain lengths and structures that are involved in ACPM interactions. It is tempting to

speculate that the overall stoichiometry of different acyl chains on ACPM may alter the interaction map, hence influencing mitochondrial function and physiology.

## CONFLICT OF INTEREST

Jaimeen D. Majmudar, Xidong Feng, Joseph F. Nabhan, Theresa Towle, Tiffany Ma, Renea Gooch, Christine Bulawa and Alain Martelli are employees of Pfizer Inc.

## ACKNOWLEDGMENTS

The Structural Genomics Consortium is a registered charity (Number 1097737) that receives funds from AbbVie, Bayer Pharma AG, Boehringer Ingelheim, Canada Foundation for Innovation, Eshelman Institute for Innovation, Genome Canada, Innovative Medicines Initiative (EU/EFPIA) [ULTRA-DD grant no. 115766], Janssen, Merck & Co., Novartis Pharma AG, Ontario Ministry of Economic Development and Innovation, Pfizer, São Paulo Research Foundation-FAPESP, Takeda, and Wellcome Trust [092809/Z/10/Z]. N.G.F. and W.W.Y. are further supported by funding from the Pfizer Rare Disease Consortium.

## REFERENCES

1. A. J. Kastaniotis, K. J. Autio, J. M. Keratar, G. Monteuuis, A. M. Makela, R. R. Nair, L. P. Pietikainen, A. Shvetsova, Z. Chen and J. K. Hiltunen, *Biochim Biophys Acta*, 2017, **1862**, 39-48.
2. J. G. Van Vranken, M. Y. Jeong, P. Wei, Y. C. Chen, S. P. Gygi, D. R. Winge and J. Rutter, *Elife*, 2016, **5**.
3. H. Angerer, S. Schonborn, J. Gorka, U. Bahr, M. Karas, I. Wittig, J. Heidler, J. Hoffmann, N. Morgner and V. Zickermann, *Biochim Biophys Acta*, 2017, **1864**, 1913-1920.
4. J. G. Van Vranken, S. M. Nowinski, K. J. Clowers, M. Y. Jeong, Y. Ouyang, J. A. Berg, J. P. Gygi, S. P. Gygi, D. R. Winge and J. Rutter, *Mol Cell*, 2018, **71**, 567-580 e564.

5. K. Fiedorczuk, J. A. Letts, G. Degliesposti, K. Kaszuba, M. Skehel and L. A. Sazanov, *Nature*, 2016, **538**, 406-410.
6. B. J. Floyd, E. M. Wilkerson, M. T. Veling, C. E. Minogue, C. Xia, E. T. Beebe, R. L. Wrobel, H. Cho, L. S. Kremer, C. L. Alston, K. A. Gromek, B. K. Dolan, A. Ulbrich, J. A. Stefely, S. L. Bohl, K. M. Werner, A. Jochem, M. S. Westphall, J. W. Rensvold, R. W. Taylor, H. Prokisch, J. P. Kim, J. J. Coon and D. J. Pagliarini, *Mol Cell*, 2016, **63**, 621-632.
7. J. Zhu, K. R. Vinothkumar and J. Hirst, *Nature*, 2016, **536**, 354-358.
8. M. T. Boniecki, S. A. Freibert, U. Muhlenhoff, R. Lill and M. Cygler, *Nat Commun*, 2017, **8**, 1287.
9. S. A. Cory, J. G. Van Vranken, E. J. Brignole, S. Patra, D. R. Winge, C. L. Drennan, J. Rutter and D. P. Barondeau, *Proc Natl Acad Sci U S A*, 2017, **114**, E5325-E5334.
10. A. Brown, S. Rathore, D. Kimanius, S. Aibara, X. C. Bai, J. Rorbach, A. Amunts and V. Ramakrishnan, *Nat Struct Mol Biol*, 2017, **24**, 866-869.
11. M. G. Herrera, M. F. Pignataro, M. E. Noguera, K. M. Cruz and J. Santos, *ACS Chem Biol*, 2018, **13**, 1455-1462.
12. D. Mellacheruvu, Z. Wright, A. L. Couzens, J. P. Lambert, N. A. St-Denis, T. Li, Y. V. Miteva, S. Hauri, M. E. Sardi, T. Y. Low, V. A. Halim, R. D. Bagshaw, N. C. Hubner, A. Al-Hakim, A. Bouchard, D. Faubert, D. Fermin, W. H. Dunham, M. Goudreau, Z. Y. Lin, B. G. Badillo, T. Pawson, D. Durocher, B. Coulombe, R. Aebersold, G. Superti-Furga, J. Colinge, A. J. Heck, H. Choi, M. Gstaiger, S. Mohammed, I. M. Cristea, K. L. Bennett, M. P. Washburn, B. Raught, R. M. Ewing, A. C. Gingras and A. I. Nesvizhskii, *Nat Methods*, 2013, **10**, 730-736.
13. S. E. Calvo, K. R. Clauser and V. K. Mootha, *Nucleic Acids Res*, 2016, **44**, D1251-1257.
14. C. L. Tsai and D. P. Barondeau, *Biochemistry*, 2010, **49**, 9132-9139.
15. F. Colin, A. Martelli, M. Clemancey, J. M. Latour, S. Gambarelli, L. Zeppieri, C. Birck, A. Page, H. Puccio and S. Ollagnier de Choudens, *J Am Chem Soc*, 2013, **135**, 733-740.

16. S. Schmucker, A. Martelli, F. Colin, A. Page, M. Wattenhofer-Donze, L. Reutenauer and H. Puccio, *PLoS One*, 2011, **6**, e16199.
17. L. K. Beilschmidt, S. Ollagnier de Choudens, M. Fournier, I. Sanakis, M. A. Hograindleur, M. Clemancey, G. Blondin, S. Schmucker, A. Eisenmann, A. Weiss, P. Koebel, N. Messaddeq, H. Puccio and A. Martelli, *Nat Commun*, 2017, **8**, 15124.
18. A. D. Sheftel, C. Wilbrecht, O. Stehling, B. Niggemeyer, H. P. Elsasser, U. Muhlenhoff and R. Lill, *Mol Biol Cell*, 2012, **23**, 1157-1166.
19. M. Sharon and C. V. Robinson, *Annu Rev Biochem*, 2007, **76**, 167-193.
20. P. C. Dorrestein, S. B. Bumpus, C. T. Calderone, S. Garneau-Tsodikova, Z. D. Aron, P. D. Straight, R. Kolter, C. T. Walsh and N. L. Kelleher, *Biochemistry*, 2006, **45**, 12756-12766.

**Table 1.** Selected protein interaction partners of ACPM identified by MS label-free quantification and filtering. Full list of hits is available in supplementary Table 1.

Protein	Other name	ID/Function
<b><i>LYRM proteins</i></b>		
C7orf55	FMC1	Assembly/stability of mitochondrial membrane ATP synthase – Complex V
NDUFB9	LYRM3	NADH dehydrogenase 1 beta subcomplex subunit 9 – Complex I
ACN9	SDHAF3	Assembly of succinate dehydrogenase (SDH) – Complex II
NDUFA6	LYRM6	NADH dehydrogenase 1 alpha subcomplex subunit 6 – Complex I
LYRM7	MZM1L	Complex III assembly factor
SDHAF1	LYRM8	Succinate dehydrogenase assembly factor 1 – Complex II
LYRM4	ISD11	Assembly/stability of cysteine desulfurase NFS1
LYRM2		unknown
<b><i>Electron transport chain</i></b>		
NDUFS1		NADH-ubiquinone oxidoreductase 75 kDa subunit – Complex I
NDUFAF5		Arginine-hydroxylase – Complex I
NDUFS7		NADH dehydrogenase [ubiquinone] iron-sulfur protein 7 – Complex I
SDHB		Succinate dehydrogenase [ubiquinone] iron-sulfur subunit – Complex II
UQCRC2		Ubiquinol-cytochrome-c reductase complex assembly factor 2 – Complex III
UQCRC1		Cytochrome b-c1 complex subunit Rieske – Complex III
ATP5H		ATP synthase subunit d – Complex V
ATPAF2		ATP synthase mitochondrial F1 complex assembly factor 2 – Complex V
<b><i>Fe-S cluster core complex</i></b>		
NFS1		Cysteine desulfurase
ISCU		Iron-sulfur cluster assembly
<b><i>Lipoylation</i></b>		
LIPT2		Transfer octanoate from octanoyl-ACPM onto lipoyl domains of lipoic acid-dependent enzymes
GLDC		Glycine cleavage system P protein – lipoic acid-dependent enzyme
<b><i>Mitochondrial fatty acid synthesis</i></b>		
OXSM		Synthesis of 3-oxoacyl-ACPM intermediates

## FIGURE LEGENDS

**Figure 1.** Log<sub>2</sub> fold changes computed from label-free quantification of the affinity-purification mass spectrometry for both biological replicates of WT ACPM IPs. Proteins meeting all thresholds and annotated as mitochondrial proteins as per MitoCarta 2.0 are labeled. Infinite fold changes (i.e. detected only in bait samples and not in control samples) were arbitrarily assigned a value of 100 (log<sub>2</sub> value of 6.64). Data were filtered as described in main text and experimental section. The complete list of interaction partners and corresponding mass spectrometry data are provided in supplementary Table 1.

**Figure 2.** Immunoprecipitation experiments in HEK293T cells. A) Representative western blots for the detection of NFS1 in inputs and after immunoprecipitation (IP) of FXN-HA, ISCU-Flag, ISD11-HA, ACPM-Flag and ACPM(S112A)-Flag using transiently transfected HEK293T cells. Non-transfected cells (NT) were used as control. HA and Flag antibodies were used to assess IP efficiency. B) Representative western blots for the detection of NFS1 and ACPM in inputs and after immunoprecipitation (IP) of FXN-HA, ISCU-Flag and ISD11-HA using transiently transfected HEK293T cells. Non-transfected cells (NT) were used as control.

**Figure 3.** Log<sub>2</sub> fold changes computed from label-free quantification of the affinity-purification mass spectrometry for averaged biological replicates of ACPM (S112A) IPs. Four biological replicates were performed for the bait samples and the control samples. The graph represents an average of two biological replicates on each axis. Proteins meeting all thresholds and annotated as mitochondrial proteins as per MitoCarta 2.0 are labeled. Infinite fold changes (i.e. detected only in bait samples and not in control samples) were arbitrarily assigned a value of 100 (log<sub>2</sub> value of 6.64). Data were filtered as described in main text and experimental section. The complete list of interaction partners and corresponding mass spectrometry data are provided in supplementary Table 3.



**Figure 4.** Knockdown experiments in HEK293T cells. Representative western blots obtained with HEK293T extracts 72 hours after transient transfection with control (NT), ACPM, ISCU and LIAS siRNAs as indicated.

**Figure 5.** ISD11-ACPM pulldown experiments in *E. coli*. A) His-ACPM and selected His-ACPM mutants were co-expressed with untagged WT ISD11 in *E. coli*. LYR/ASA corresponds to substitutions of residues L12, Y13 and R14 with alanine, serine and alanine residues, respectively. The presence of ISD11 in inputs and elution fractions was detected by coomassie blue staining and immunoblotting (IB). B) His-ACPM was co-expressed with WT ISD11 or selected ISD11 mutants (untagged) in *E. coli*. The presence of ISD11 in inputs and elution fractions was detected by coomassie blue staining and immunoblotting (IB).

**Figure 6.** Native ESI mass spectrum of ACPM-ISD11 recombinant complex. A) A mixture of ACPM monomer, ACPM-ISD11 heterodimer and tetramer detected with broad peak due to ACPM heterogeneity. B) Expanded spectrum corresponding to ACPM-ISD11 heterodimer

**Figure 7.** Identification of 4'-PP acyl chains in the ACPM-ISD11 recombinant complex. A) MS/MS/MS spectra of ejected 4'-PP conjugated acyl-chains with both parent and fragment ions detected with ppm mass accuracy. B) Proposed structures of 4'-PP conjugated acyl-chains on ACPM. C) Mapping of the simulated isotopic distributions (black) of holo-ACPM over observed data (red) provided another strong evidence for the proposed 4'-PPT conjugated acyl-chain structures.

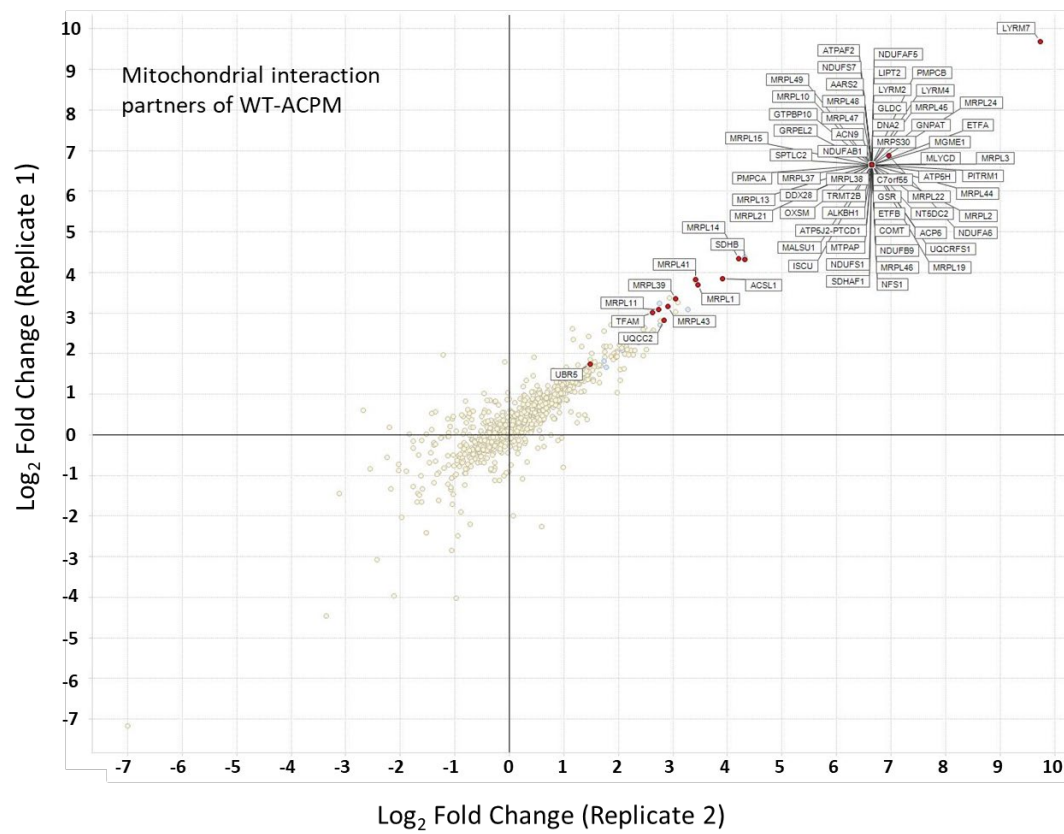


**Figure 1**

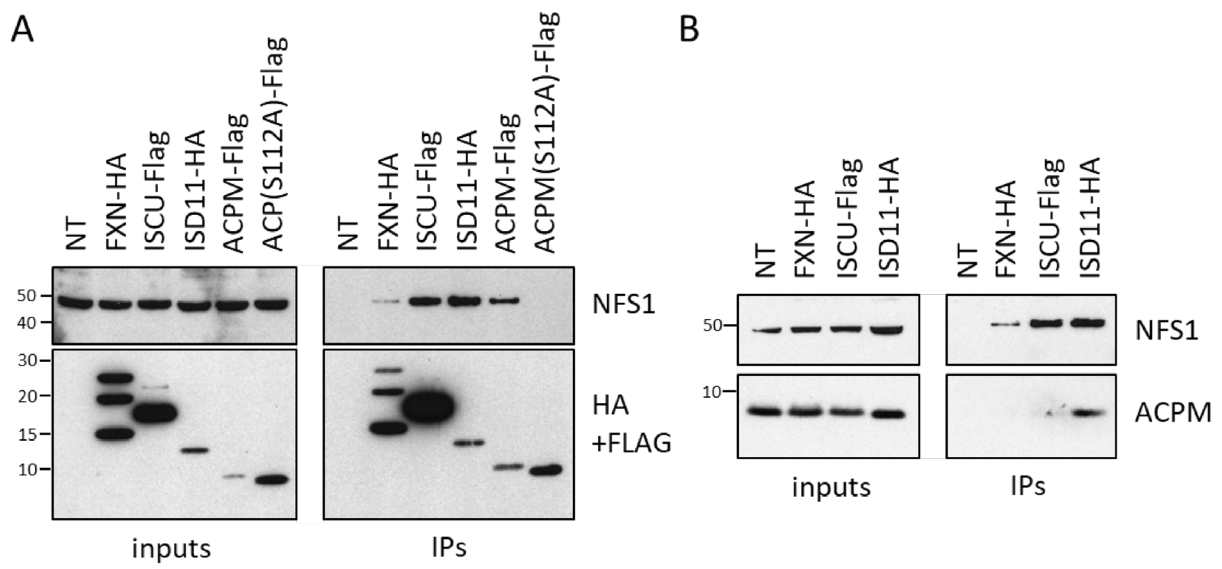


**Figure 2**

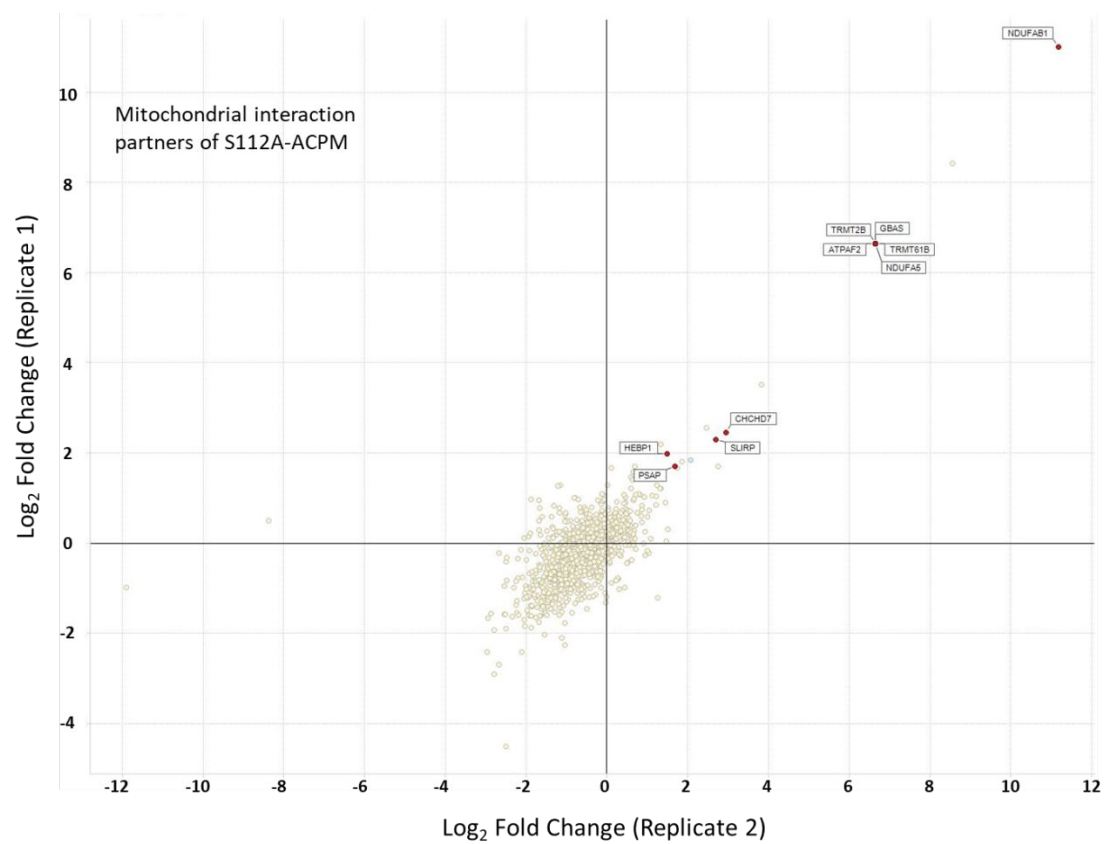


**Figure 3**

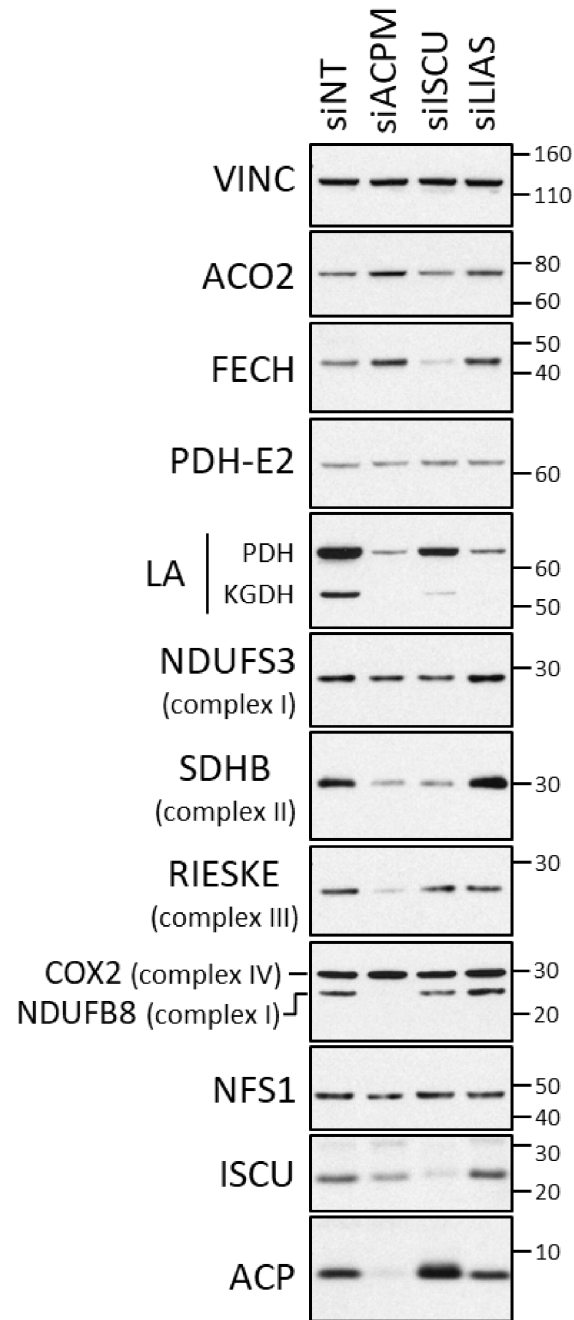


**Figure 4**

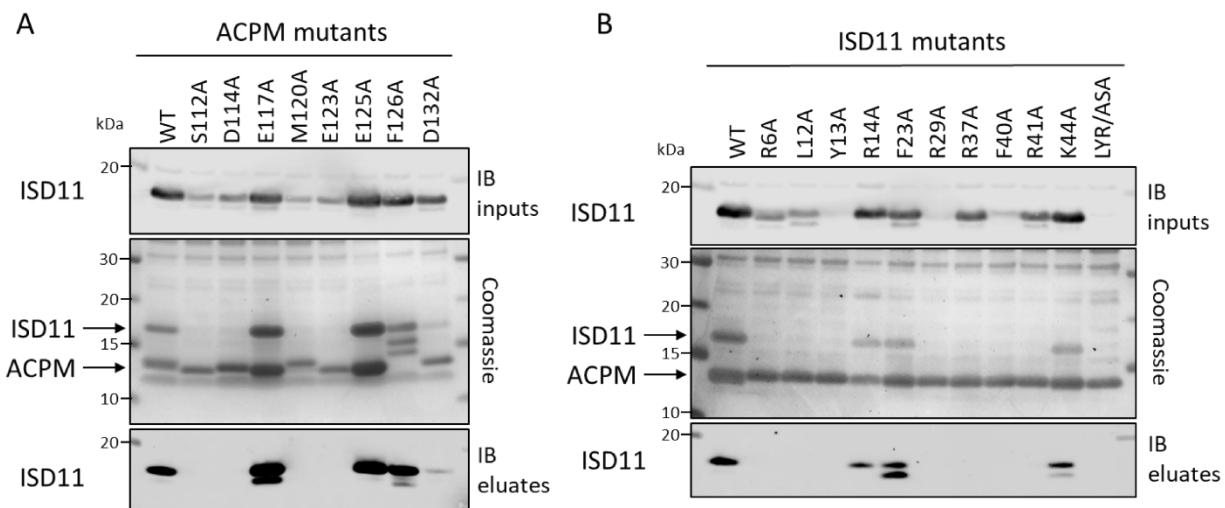


**Figure 5**

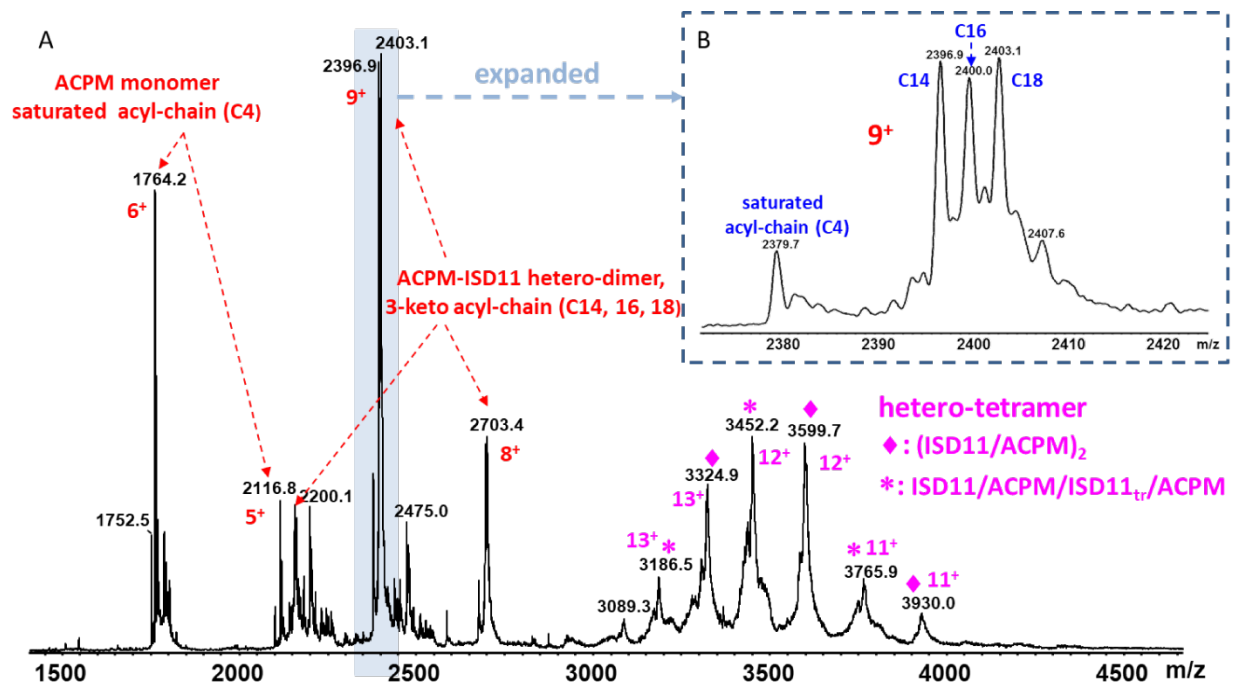


Figure 6

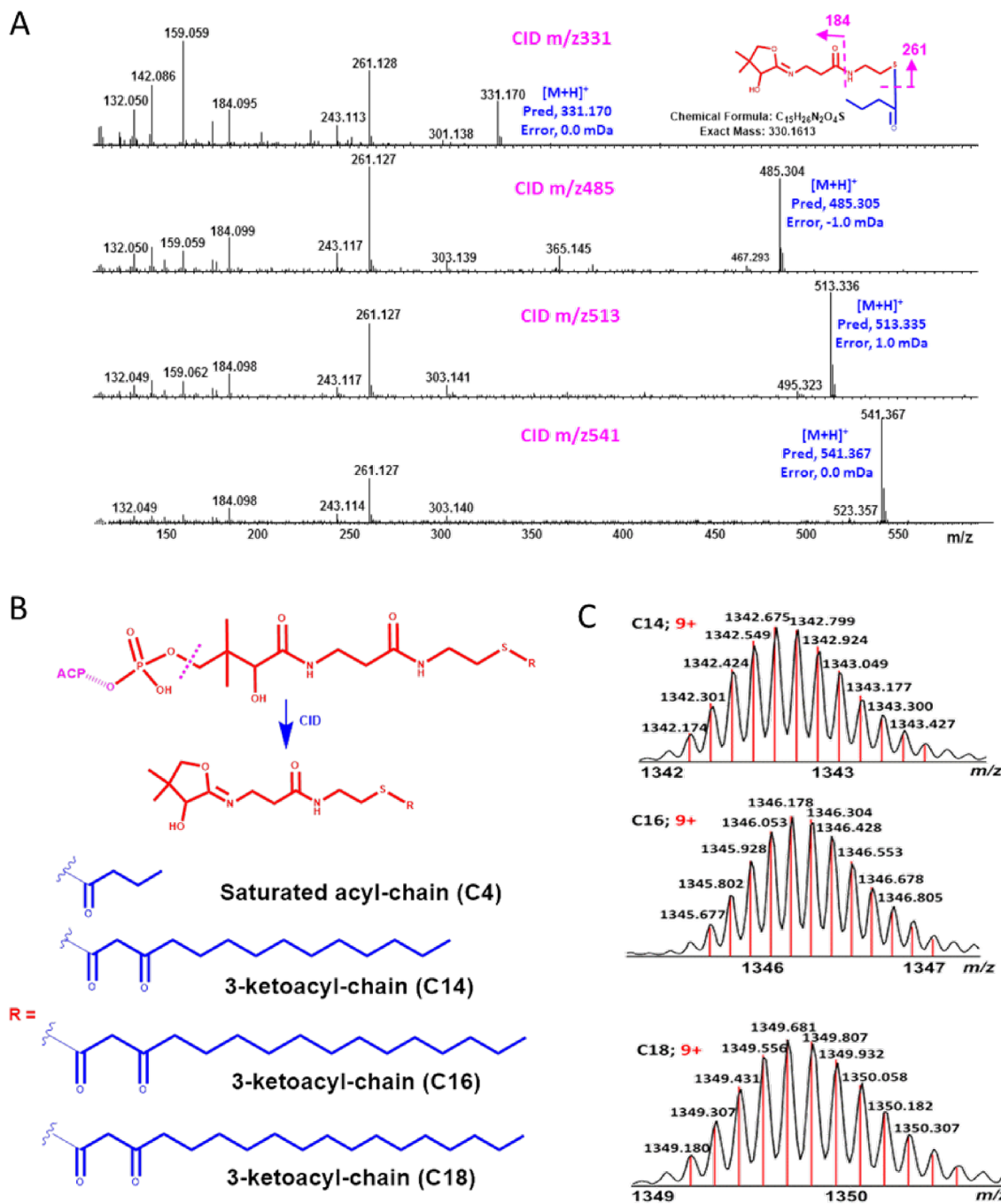


Figure 7